Photothermal effect and cytotoxicity of CuS nanoflowers deposited over folic acid conjugated nanographene oxide

Gururaj M. Neelgund*[a], Aderemi Oki*[a], Subhani Bandara[b] and Laura Carson[b]

[a]*Department of Chemistry, Prairie View A&M University, Prairie View, TX 77446, United States*

[b]*Cooperative Agricultural Research Center, Prairie View A&M University, Prairie View, TX 77446, United States*

Preparation of diazonium salt

Sulfanilic acid (200 mg) and sodium nitrite (75 mg) were dissolved in 50 mL of 0.25% sodium hydroxide solution, and it was slowly added to 50 mL of 0.1N hydrochloric acid. The resulting mixture was stirred in ice bath for 2hr and stored in refrigerator for overnight, centrifuged and washed with DI water to form GO-SO_3H.

Calculation of photothermal transduction efficiency (η) according

To calculate the value of *hS*, a dimensionless driving force of temperature, θ is introduced and scaled using the maximum system temperature, T_{max} and the surrounding temperature, T_{surr}.

$$\theta = \frac{T - T_{surr}}{T_{max} - T_{surr}} \qquad (2)$$

and the sample system time constant, τs was evaluated using the following equation (3)

$$t = -\tau s \ln(\theta) \qquad (3)$$

The value of τs was calculated by Figs. S10 and S11, and using its value, the unknown parameter, *hS* was evaluated with the help of following equation (4).

$$hS = \frac{m_D C_D}{\tau s} \qquad (4)$$

where m_D is mass of DI water (1.01g) and C_D is its heat capacity. The value of Q_{dis} was measured separately using quartz cuvette containing only DI water without any sample and it was found to be 25.9 mW.

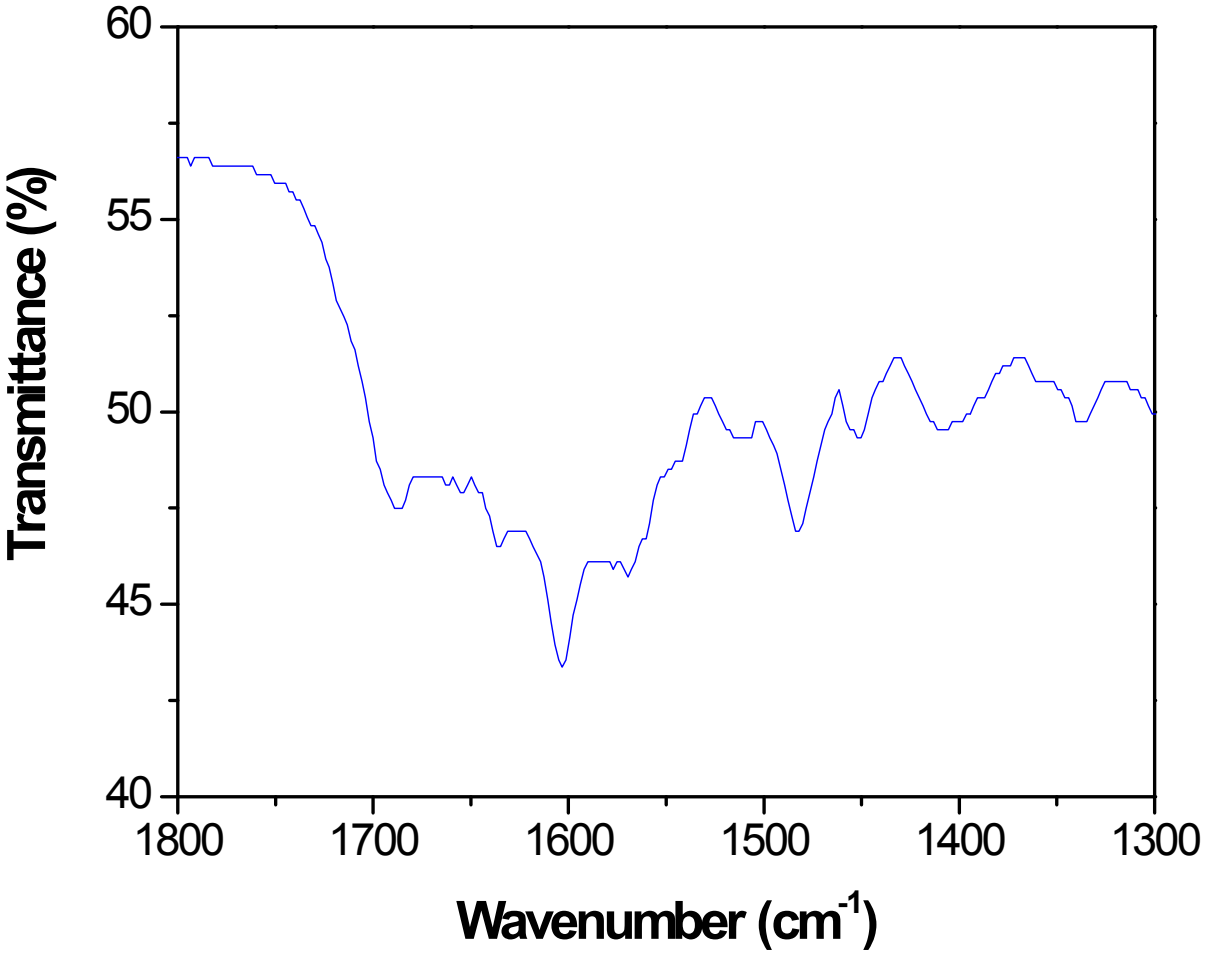

Fig. S1. ATR-FTIR spectrum of NGO-FA in specified region.

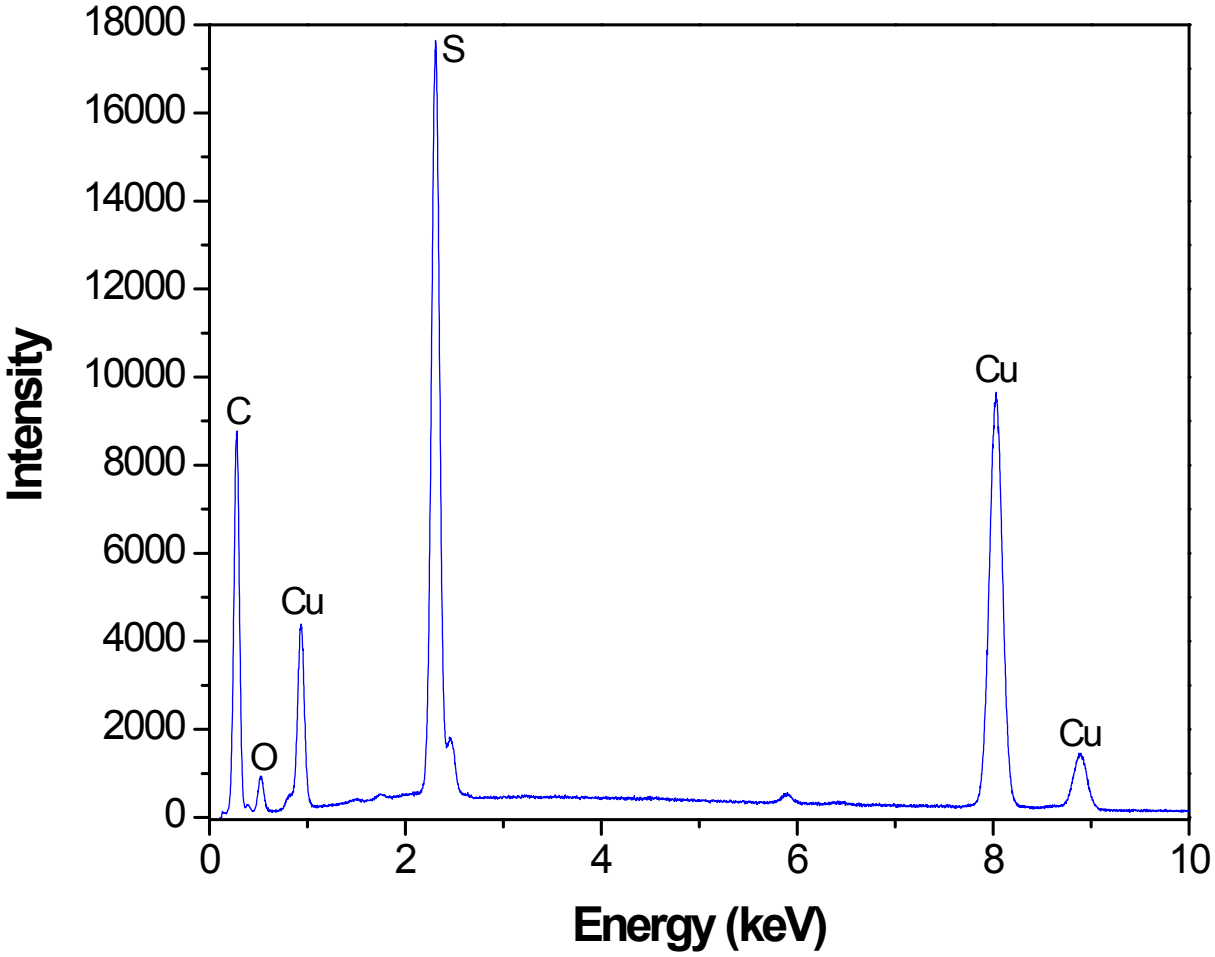

Fig. S2. EDS of NGO-FA-CuS.

Table S1. Photothermal efficiency *(η)* value reported for popular CuS and Au contained photothermal agents.

Sample	Reported value of photothermal efficiency (%)	Reference
NGO-FA-CuS	46.2	This work
CuS nanoflowers	38.4	This work
CuSCs-PEG-FA	27.4	S1
Cys-CuS NPs	27.4	S2
HCuS@Cu_2S@Au	35.0	S3
CuS nanodiamonds	36.4	S4
Au nanoshells	18.0	S5
Au nanorods	22.0	S6
$Cu_{2-x}Se$ nanoparticles	22.0	S7
Au nanoshells	25.0	S8
Cu_9S_5 nanoparticles	25.7	S9
Au vesicle	18.0	S10

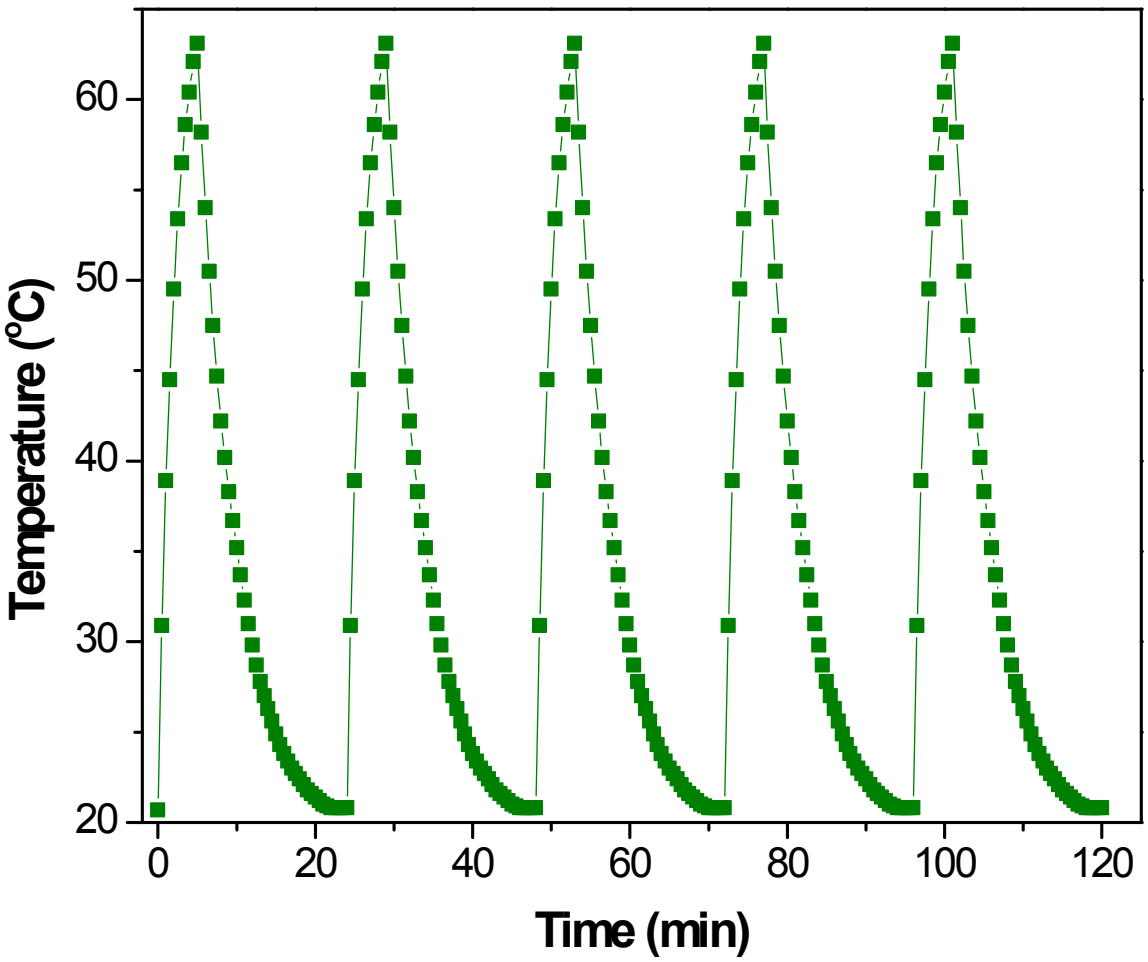

Fig. S3. Temperature variation measured for the aqueous dispersion of NGO-FA-CuS (1 mg/mL) for five cycles under illumination by a 980 nm laser.

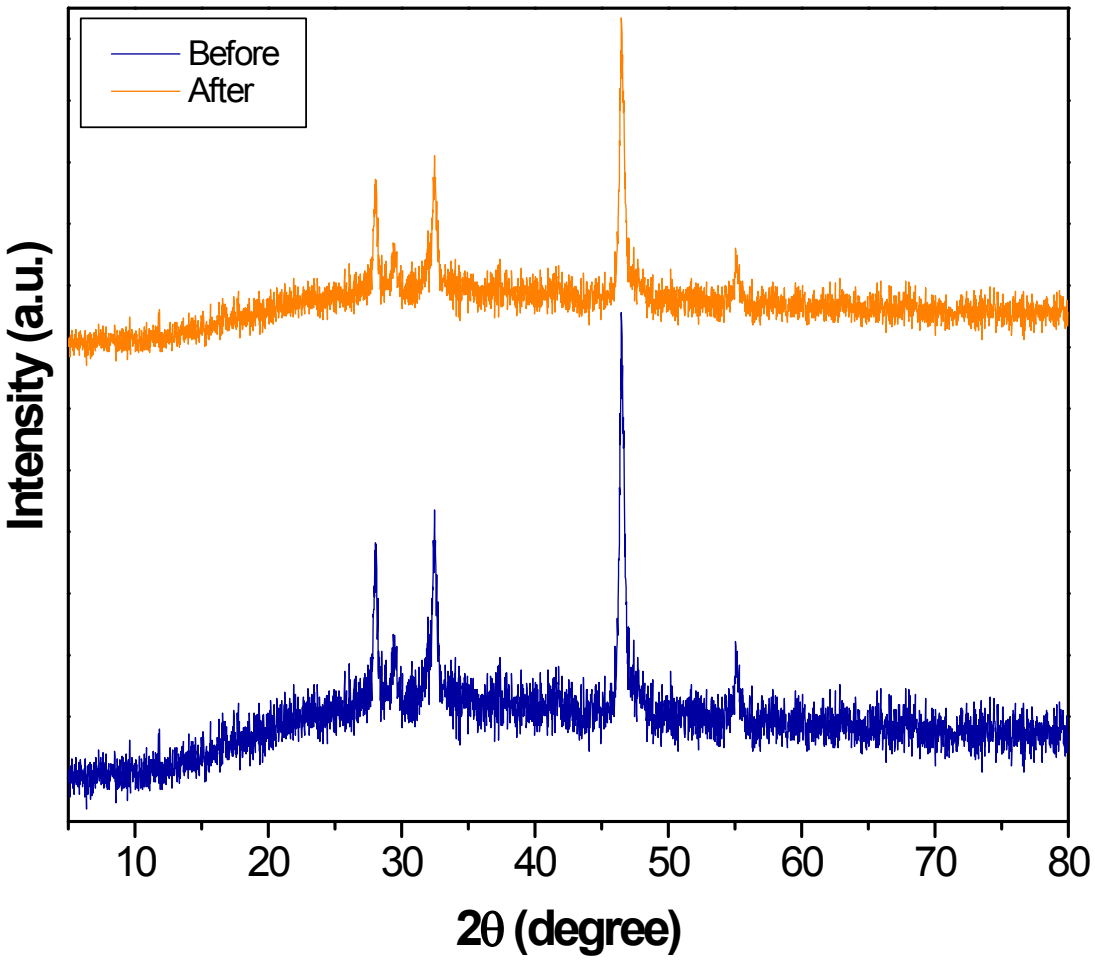

Fig. S4. XRD patterns of NGO-FA-CuS before and after applying in five successive cycles of photothermal effect.

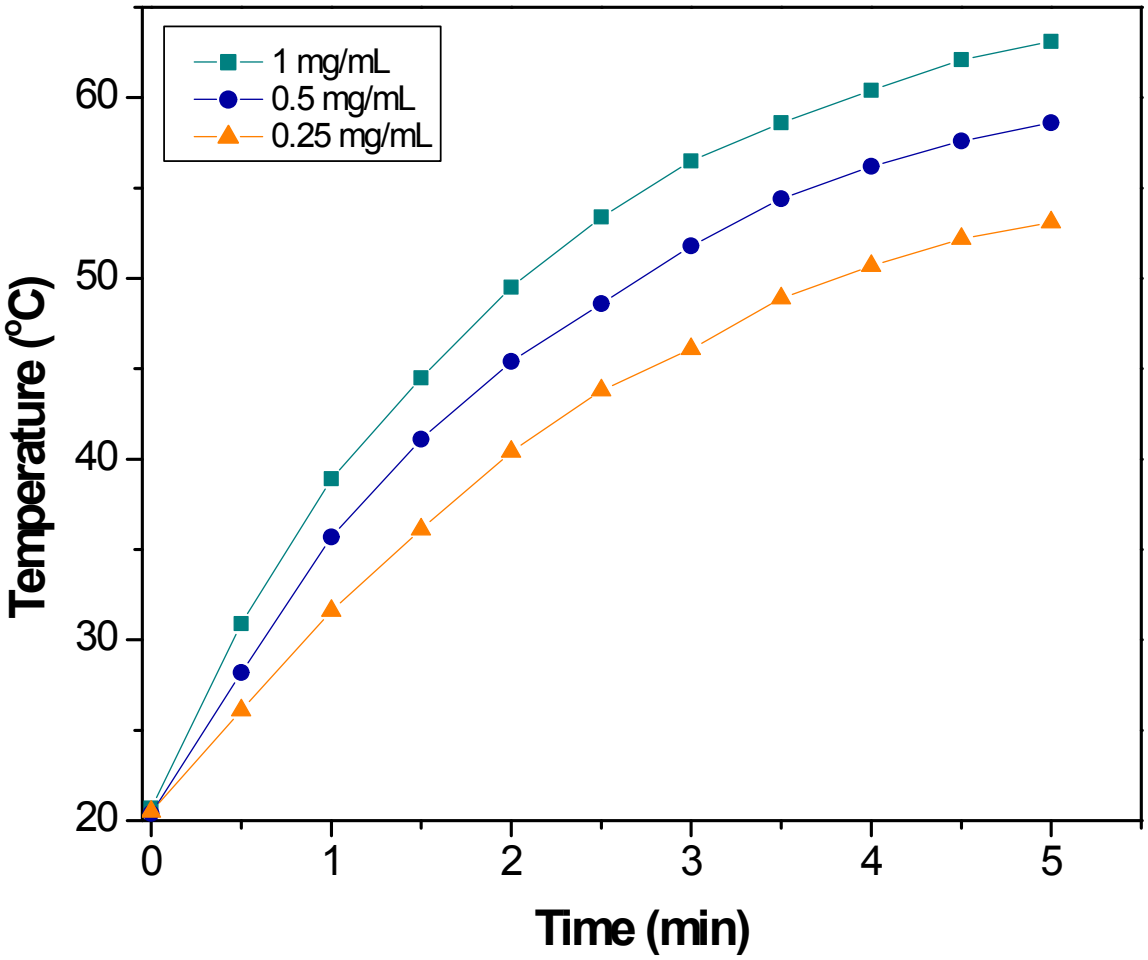

Fig. S5. Photothermal effect of NGO-FA-CuS measured at different concentrations under illumination to 980 nm laser.

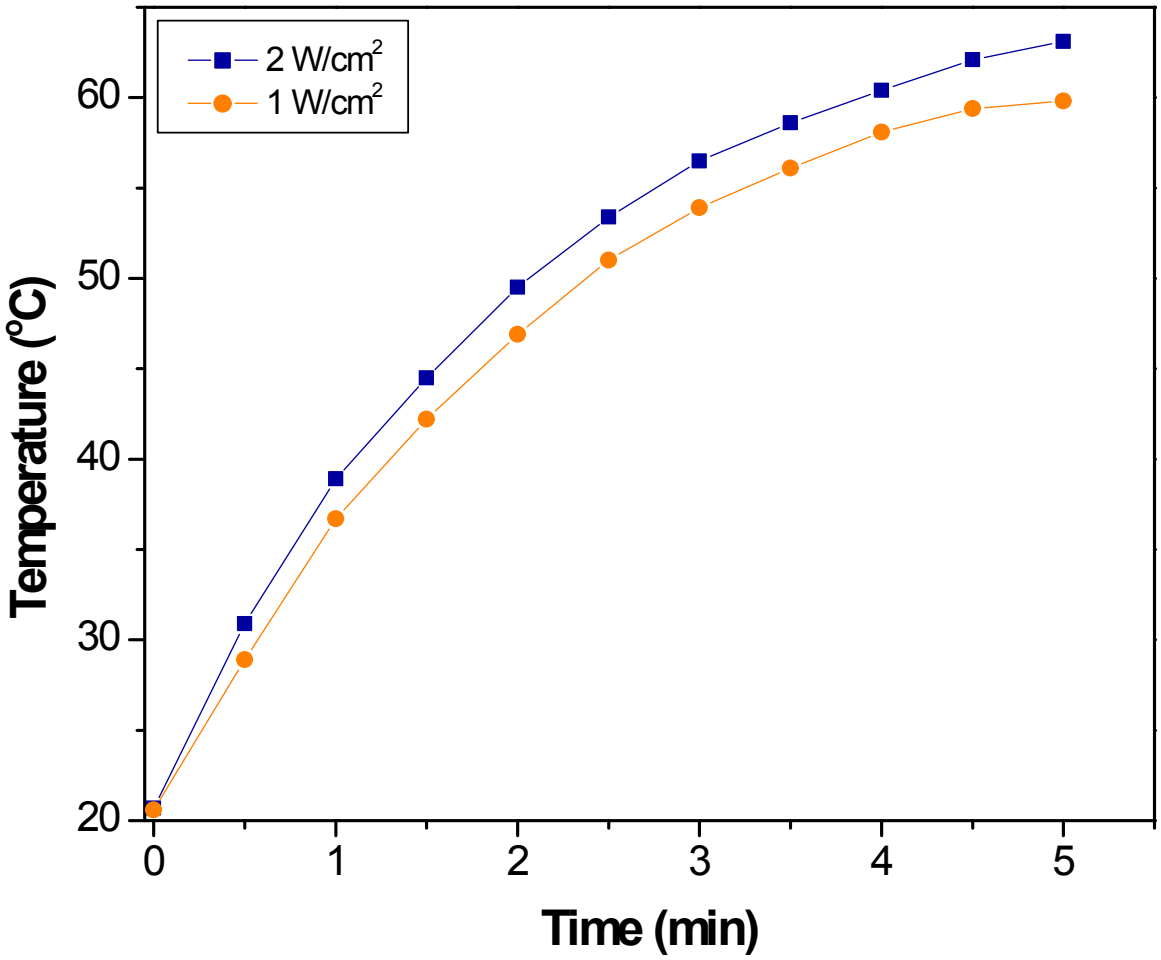

Fig. S6. Photothermal effect of NGO-FA-CuS measured at 1 and 2 W/cm^2 under illumination to 980 nm laser.

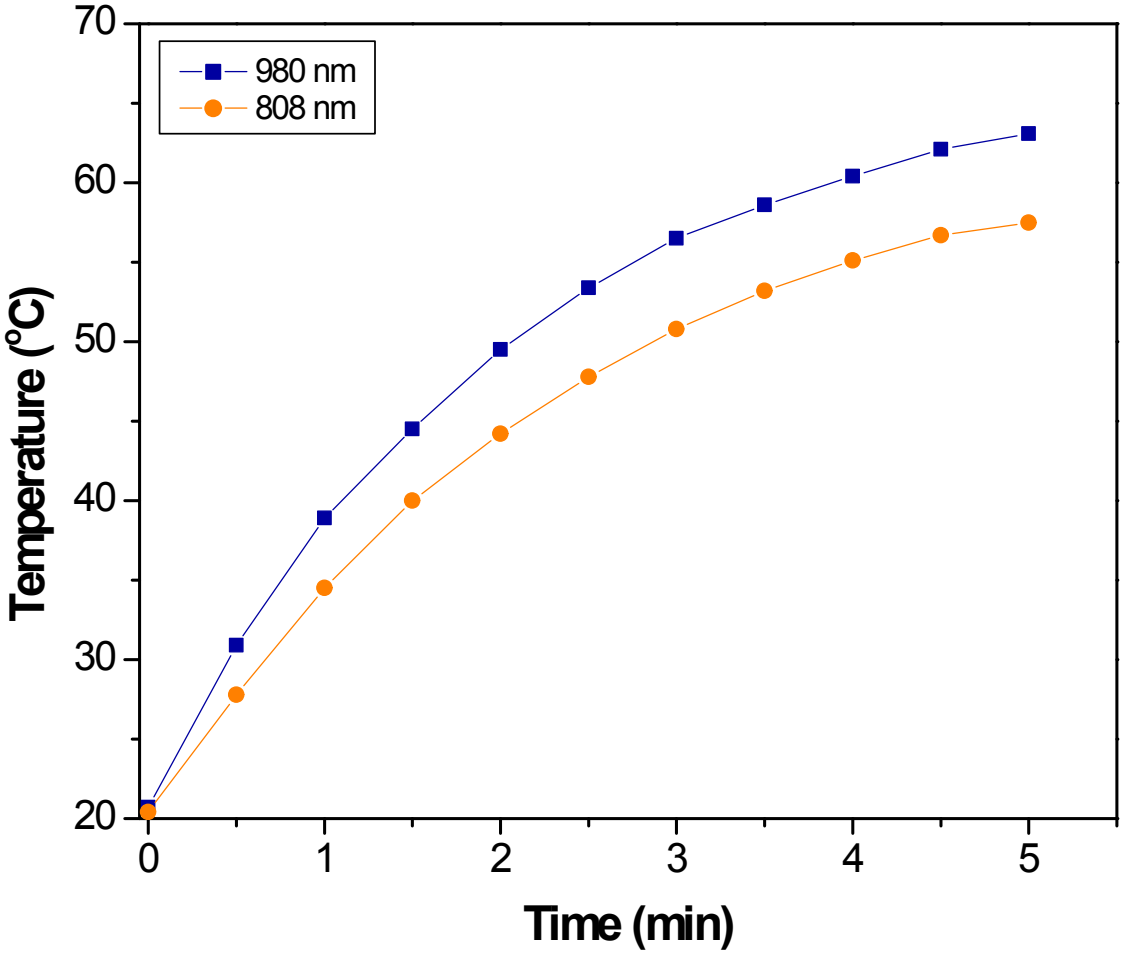

Fig. S7. Photothermal effect of NGO-FA-CuS measured under illumination to 808 and 980 nm laser.

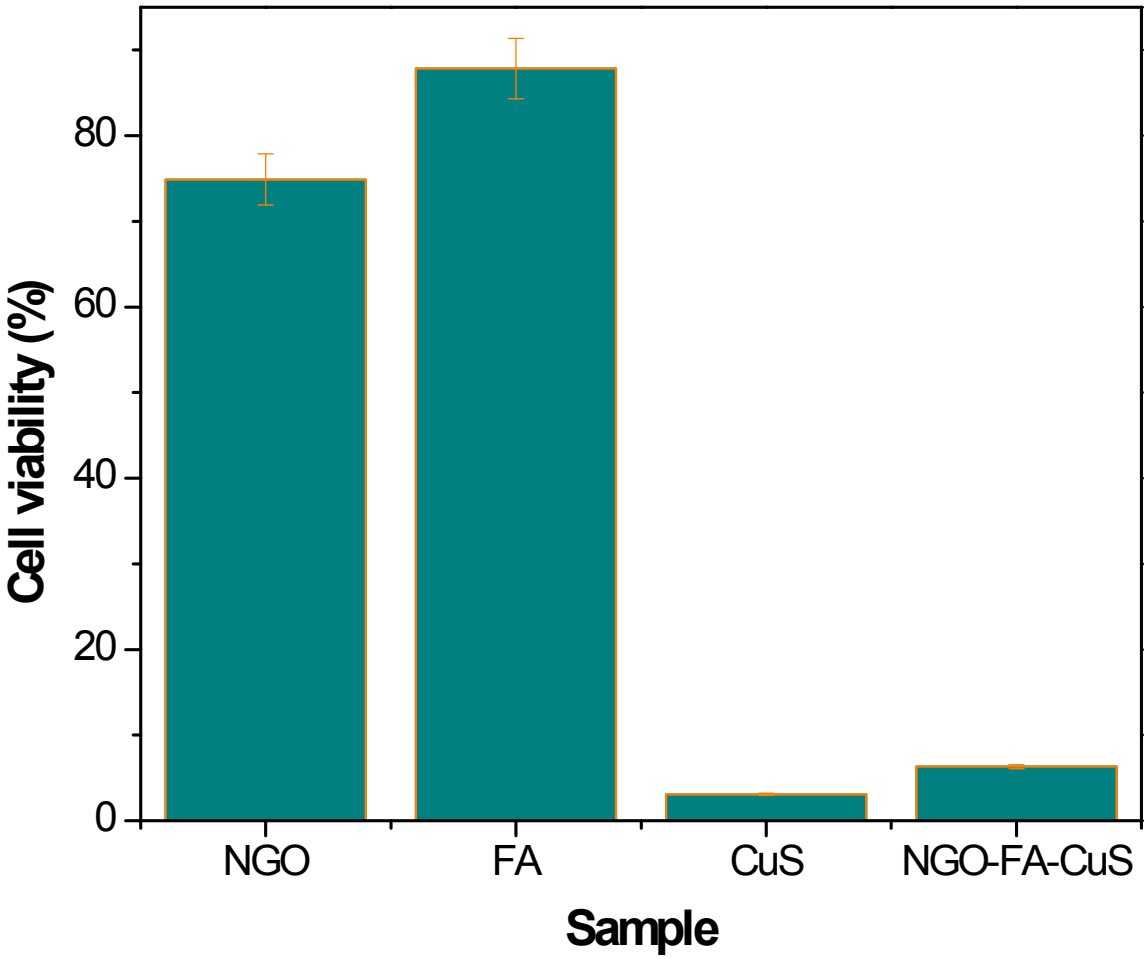

Fig. S8. Cytotoxicity of NGO-FA-CuS measured for HeLa cells at concentration of 200 μg/mL.

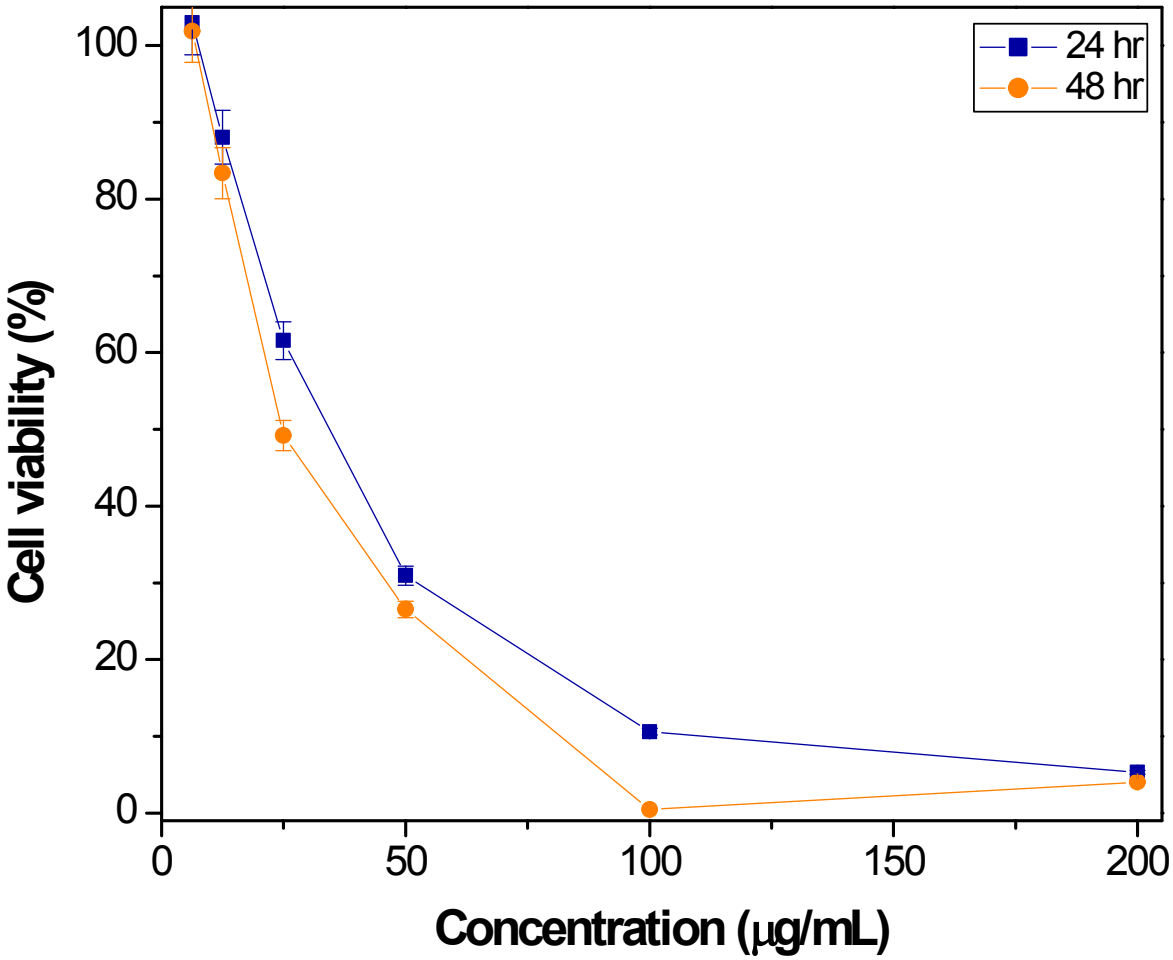

Fig. S9. Cytotoxicity of NGO-FA-CuS over KB cells at different incubation time.

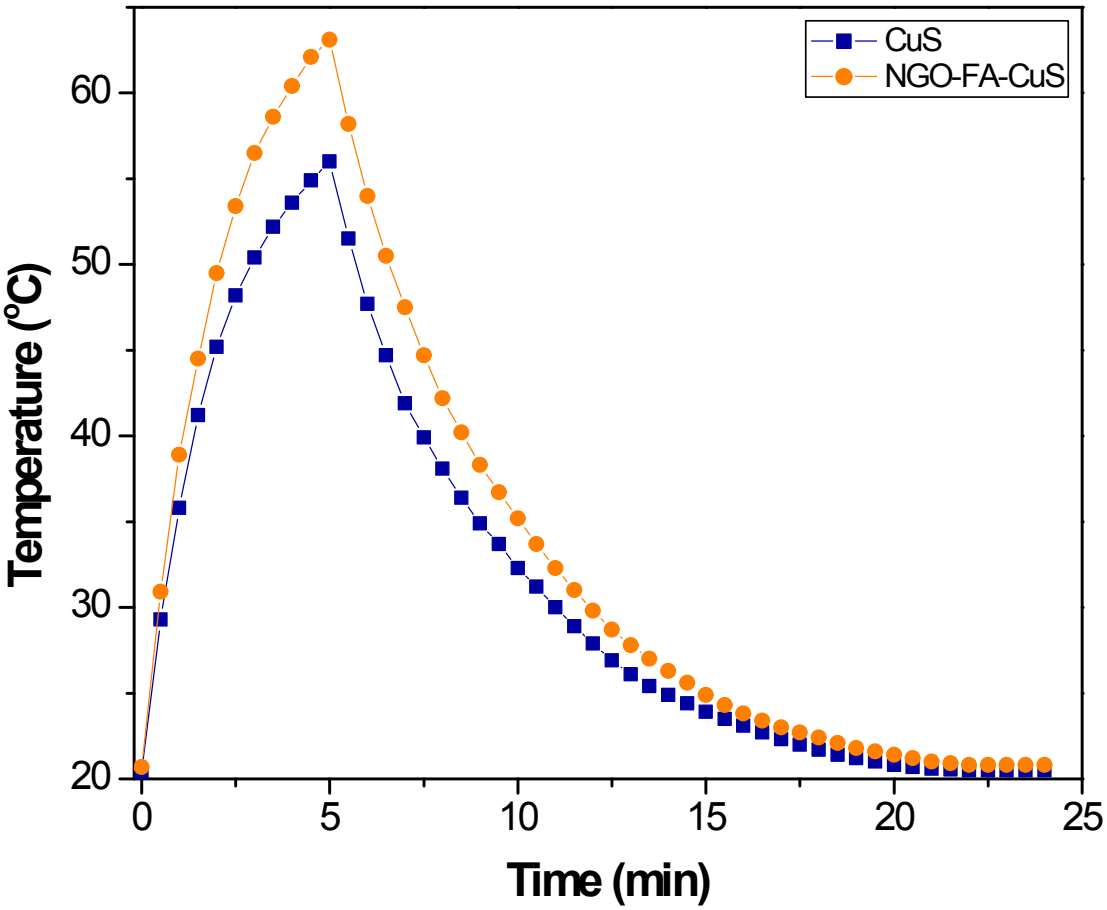

Fig. S10. Temperature variation found for aqueous dispersion of Cus and NGO-FA-CuS under exposure to 980 nm laser followed by its shut off.

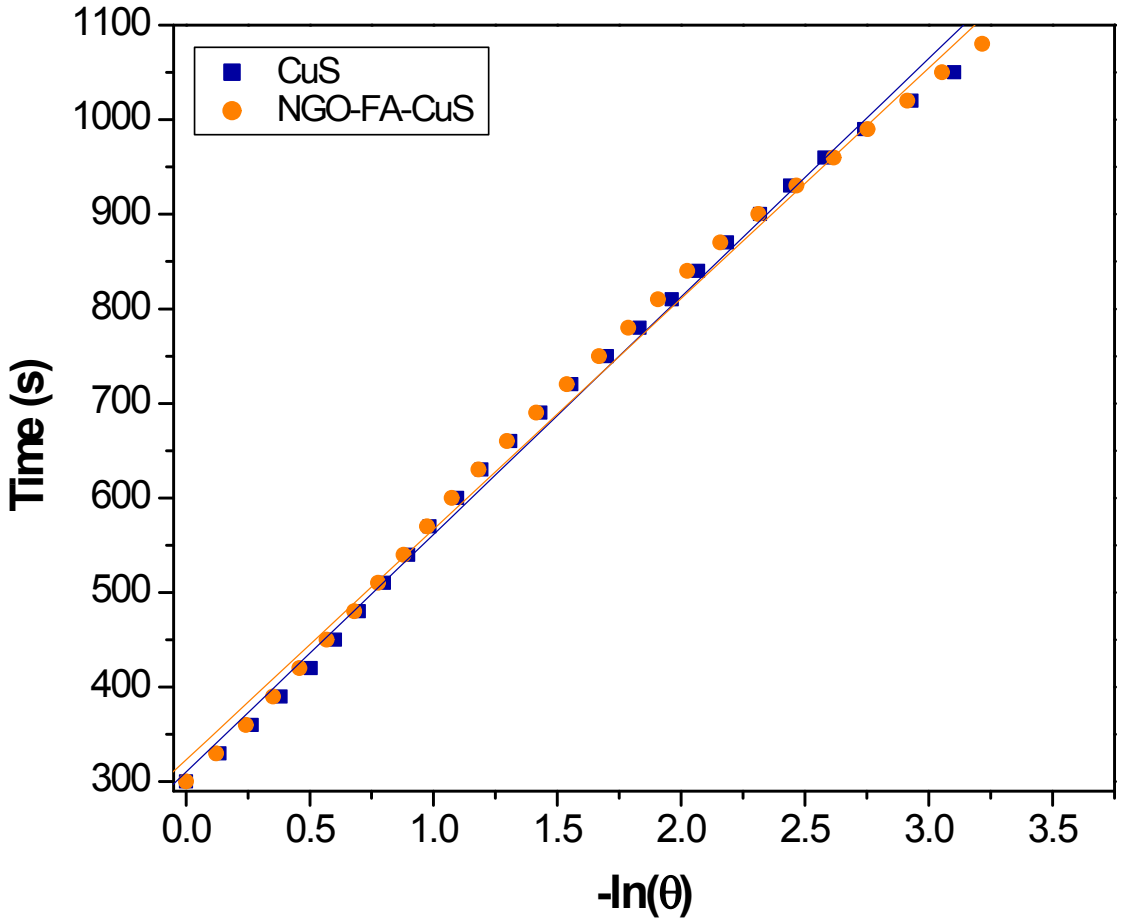

Fig. S11. The plot of time from cooling period versus negative natural logarithm of driving force temperature obtained for Cus and NGO-FA-CuS using the data shown in Fig. S10.

References

S1 M. Xu, G. Yang, H. Bia, J. Xu, L. Feng, D. Yang, Q. Sun, S. Gai, F. He, Y. Dai, C. Zhong and P. Yang, Combination of CuS and g-C_3N_4 QDs on upconversion nanoparticles for targeted photothermal and photodynamic cancer therapy, *Chem. Eng. J.,* 2019, 360, 866–878.

S2 X. Liu, B. Li, F. Fu, K. Xu, R. Zou, Q. Wang, B. Zhang, Z. Chen and J. Hu, Facile synthesis of biocompatible cysteine-coated CuS nanoparticles with high photothermal conversion efficiency for cancer therapy, *Dalton Trans.,* 2014, 43**,** 11709-11715.

S3 X. Deng, K. Li, X. Cai, B. Liu, Y. Wei, K. Deng, Z. Xie, Z. Wu, P. Ma, Z. Hou, Z. Cheng and J. Lin, A hollow-structured CuS@Cu2S@Au nanohybrid: synergistically enhanced photothermal efficiency and photoswitchable targeting effect for cancer theranostics, *Adv. Mater.,* 2017, 29, 1701266.

S4 Y. Qiao, Y. Ping, H. Zhang, B. Zhou, F. Liu, Y. Yu, T. Xie, W. Li, D. Zhong, Y. Zhang, K. Yao, H. A. Santos and M. Zhou, Laser-activatable CuS nanodots to treat multidrug-resistant bacteria and release copper ion to accelerate healing of infected chronic nonhealing wounds, *ACS Appl. Mater. Interfaces,* 2019, 11, 3809−3822.

S5 P. Huang, J. Lin, W. Li, P. Rong, Z. Wang, S. Wang, X. Wang, X. Sun, M. Aronova, G. Niu, R. D. Leapman, Z. Nie and X. Chen, Biodegradable gold nanovesicles with an ultrastrong plasmonic coupling effect for photoacoustic imaging and photothermal therapy, *Angew. Chem. Int. Ed.,* 2013, 52, 13958-13964.

S6 C. M. Hessel, V. P. Pattani, M. Rasch, M. G. Panthani, B. Koo, J. W. Tunnell and B. A. Korgel, Copper selenide nanocrystals for photothermal therapy, *Nano Lett.* 2011, 11, 2560-2566.

S7 V. P. Pattani, J. W. Tunnell, Nanoparticle-mediated photothermal therapy: a comparative study of heating for different particle types, *Lasers Surg. Med.,* 2012, 44, 675-684.

S8 Q. Tian, F. Jiang, R. Zou, Q. Liu, Z. Chen, M. Zhu, S. Yang, J. Wang, J. Wang, J. Hu, Hydrophilic Cu_9S_5 nanocrystals: a photothermal agent with a 25.7% heat conversion efficiency for photothermal ablation of cancer cells in vivo, *ACS Nano*, 2011, 5, 9761-9771.

S9 E. Ju, K. Dong, Z. Liu, F. Pu, J. Ren, X. Qu, Tumor microenvironment activated photothermal strategy for precisely controlled ablation of solid tumors upon NIR irradiation, *Adv. Funct. Mater.,* 2015, 2, 1574-1580.

S10 P. Huang, J. Lin, W. Li, P. Rong, Z. Wang, S. Wang, X. Wang, X. Sun, M. Aronova, G. Niu, R. D. Leapman, Z. Nie, X. Chen, Biodegradable gold nanovesicles with an ultrastrong plasmonic coupling effect for photoacoustic imaging and photothermal iherapy, *Angew. Chem. Int. Ed.,* 2013, 52, 13958-13964.